Rapidly Prepared Nanocellulose Hybrids as Gas Barrier, Flame Retardant, and Energy Storage Materials

ACS APPLIED NANO MATERIALS

www.acsanm.org

Article

Rapidly Prepared Nanocellulose Hybrids as Gas Barrier, Flame Retardant, and Energy Storage Materials

Yunus Can Gorur,* Hugo S. Francon, Jatin Sethi, Lorenza Maddalena, Céline Montanari, Michael S. Reid, Johan Erlandsson, Federico Carosio, Per A. Larsson, and Lars Wågberg*

Cite This: *ACS Appl. Nano Mater.* 2022, 5, 9188–9200

Read Online

ACCESS | Metrics & More | Article Recommendations | Supporting Information

ABSTRACT: Cellulose nanofibril (CNF) hybrid materials show great promise as sustainable alternatives to oil-based plastics owing to their abundance and renewability. Nonetheless, despite the enormous success achieved in preparing CNF hybrids at the laboratory scale, feasible implementation of these materials remains a major challenge due to the time-consuming and energy-intensive extraction and processing of CNFs. Here, we describe a scalable materials processing platform for rapid preparation (<10 min) of homogeneously distributed functional CNF–gibbsite and CNF–graphite hybrids through a pH-responsive self-assembly mechanism, followed by their application in gas barrier, flame retardancy, and energy storage materials. Incorporation of 5 wt % gibbsite results in strong, transparent, and oxygen barrier CNF–gibbsite hybrid films in 9 min. Increasing the gibbsite content to 20 wt % affords them self-extinguishing properties, while further lowering their dewatering time to 5 min. The strategy described herein also allows for the preparation of freestanding CNF–graphite hybrids (90 wt % graphite) that match the energy storage performance (330 mA h/g at low cycling rates) and processing speed (3 min dewatering) of commercial graphite anodes. Furthermore, these ecofriendly electrodes can be fully recycled, reformed, and reused while maintaining their initial performance. Overall, this versatile concept combines a green outlook with high processing speed and material performance, paving the way toward scalable processing of advanced ecofriendly hybrid materials.

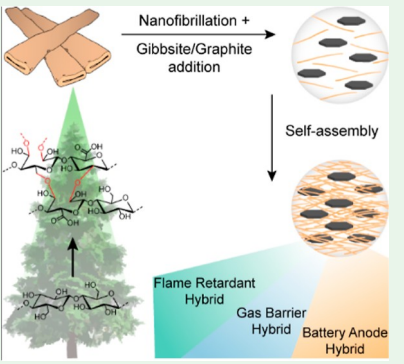

KEYWORDS: *functional hybrids, nanocomposites, CNF, self-assembly, green materials, gibbsite*

INTRODUCTION

The fight against global warming calls for the development of novel materials with low ecological footprint that can perform on par with or better than their traditional counterparts. However, scalable implementation of these new materials remains a critical challenge due to inferior material properties and long processing times. Solving these problems demands versatile material processing platforms, through which incorporation of sustainable materials can be readily achieved. Employing a multi-component approach can help address these challenges by providing renewable hybrid materials with functionalities that would otherwise not be possible.[1,2]

Hybrid materials commonly refer to a sub-section of composites that have nanoscale constituents.[3] Hybrid structures are promising because their small building blocks and high specific surface area allow us to tune nanoscale properties in order to obtain ideal macro-scale performance. In nature, this is achieved through a slow but effective bottom-up assembly of the constituents, where the association is a balance between entropically driven interactions and different opposing forces that allow for the growth of ideally packed ordered materials,[4−6] of which nacre is a great example.[7] While nacre has excellent properties, its slow growth is difficult to scale and thus alternative assembly methods for high-performance sustainable hybrid materials are needed. This means that the ideal processing method for designing sustainable hybrids must be fast, yet ensure a homogeneous component distribution.

Aside from being the main building block of the wood fiber wall, cellulose nanofibrils (CNFs) also possess dispersive properties[8] and a natural tendency to form strong networks,[9] making them an ideal component for preparing green functional hybrid structures.[10] CNFs have previously been used in combination with other components such as clays or carbons to prepare hybrids with different functionalities such as gas barrier,[11,12] flame retardancy,[13,14] and energy storage.[8,15] Despite their exciting properties, there are unresolved challenges in transitioning these hybrid materials from research to commercial adoption. These challenges are mainly related to CNFs' time-consuming and energy-intensive production and processing into dry materials (i.e., costly CNF extraction and slow water removal).[16−18] We have recently demonstrated a

Received: April 8, 2022
Accepted: June 7, 2022
Published: June 21, 2022

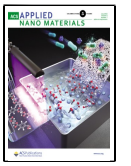

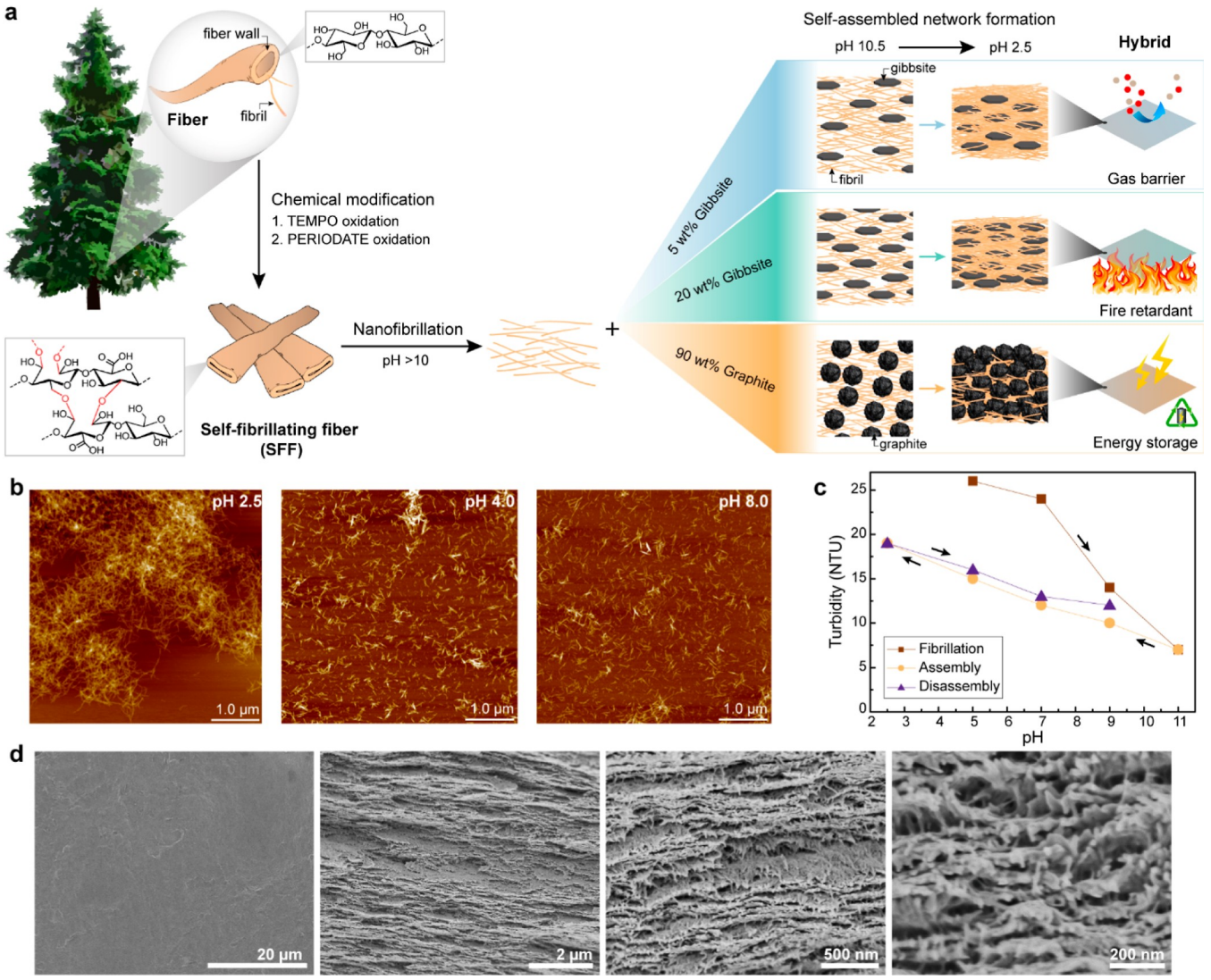

Figure 1. (a) Schematic image showing the chemistry of SFFs, their facile nanofibrillation and self-assembly to obtain hybrids with different functionalities. (b) Atomic force microscopy (AFM) images of CNFs adsorbed onto silica surfaces at different pH values to illustrate the pH-responsive self-assembly of the CNFs. (c) Turbidity as a function of pH for visually monitoring the self-fibrillation of SFFs and the pH-responsive reversible self-assembly of the resulting CNFs. (d) Scanning electron microscopy (SEM) images showing the homogeneous smooth surface (left) and the nanoscale internal structure (middle two and right) of the CNF nanopapers (i.e., CNFs only) prepared using self-fibrillation and the subsequent pH-responsive self-assembly.

two-step oxidation of cellulose fibers in aqueous media that can yield self-fibrillating fibers (SFFs).[19,20] Using SFFs, CNFs can be liberated and processed into nanopapers simultaneously via an increase in pH (≥pH 10). These SFF-based CNFs are pH-responsive and self-associative in a reversible manner due to their surface carboxyl and aldehyde groups. This concept can be combined with other materials during the self-assembly for a rapid bottom-up processing of green hybrid structures. Consequently, SFFs can be useful as a hybrid component because they allow facile nanofibrillation and nanoscale tailoring of interactions with other functional constituents. Gibbsite and graphite are interesting nanoscale components for preparing ecofriendly cellulose-based hybrid structures because of their morphology and versatile functionalities such as fire retardancy and energy storage, respectively.[21,22]

Gibbsite is an interesting pH-responsive material that together with CNFs can form hybrids with flame retardant or gas barrier functionalities.[23] Gibbsite exhibits an isoelectric point at pH = 10, above which its surface charge is reversed from positive to negative.[24,25] This attribute can be useful in tailoring CNF−gibbsite interactions in the preparation of flame retardant CNF hybrids with layered nanostructures. Moreover, gibbsite is abundant and industrially relevant as an important part of aluminum production.[26] These features make CNF−gibbsite hybrids ideal candidates as bio-based flame retardants with a lower environmental impact compared to their expensive commercially available polymeric equivalents.[27]

Graphite is another attractive component for CNF hybrids, as it is the material of choice for state-of-the-art anodes in Li-ion batteries. Graphite is inexpensive, safe, and abundant, which makes it a promising functional component that can provide the CNF hybrids with energy storage properties.[28,29] Because commercial anodes require a high loading of graphite (>90 wt %), their preparation relies on the use of binders to ensure their mechanical and structural integrity. Common commercial binders such as carboxymethylcellulose (CMC)

https://doi.org/10.1021/acsanm.2c01530
ACS Appl. Nano Mater. 2022, 5, 9188−9200

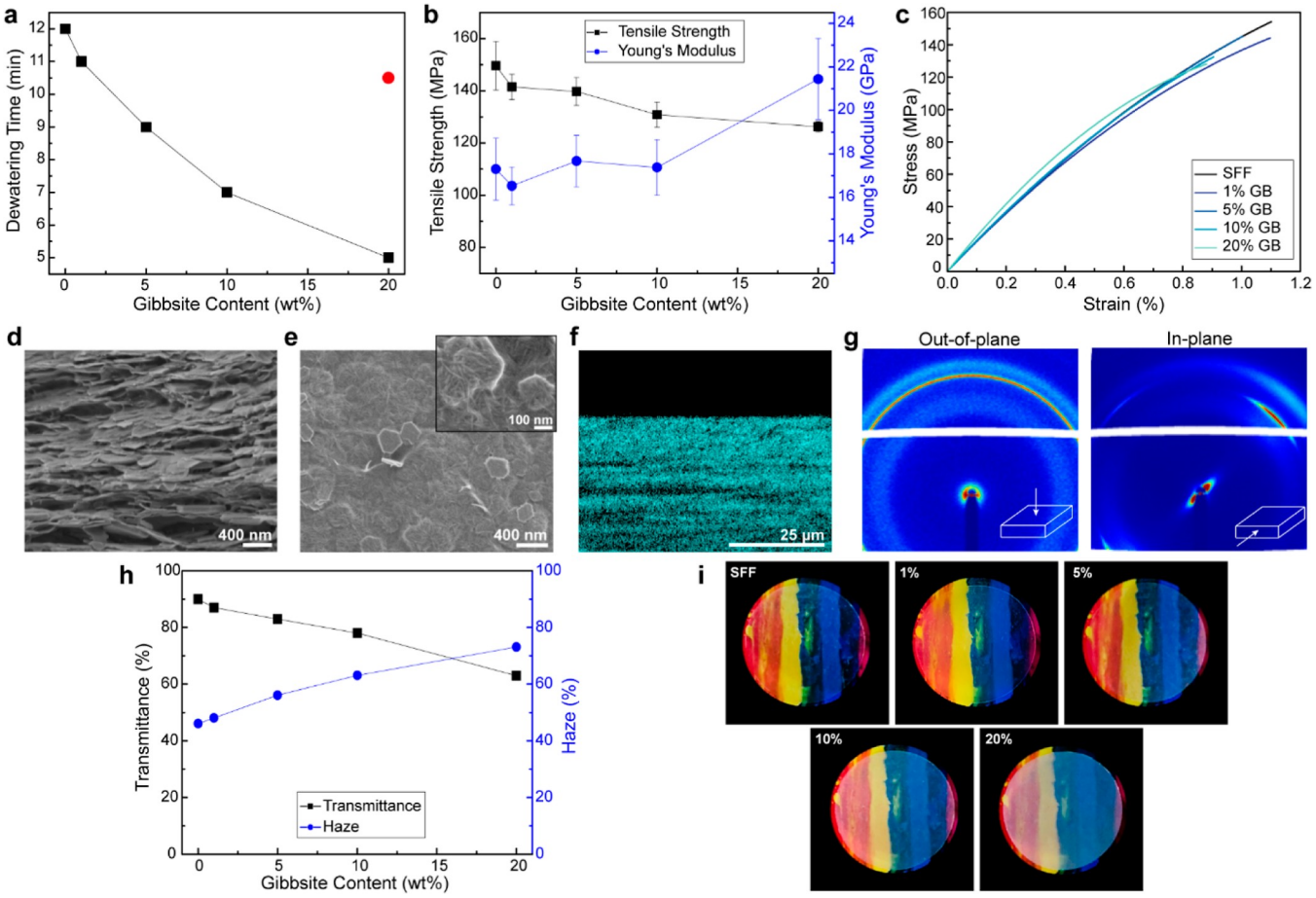

Figure 2. (a) Dewatering time of the CNF hybrids at pH = 2.5 with respect to gibbsite content, the red circle represents the dewatering time of SFF80−GB0 (formulation without the added gibbsite). (b) Tensile strength and Young's modulus values for the hybrid films as a function of the gibbsite content. (c) Representative stress−strain curves of the hybrid films with varying gibbsite content. (d) Cross-sectional SEM micrograph of the SFF90−GB10 sample showing the layered hybrid structure. (e) Top-view SEM image of the SFF90−GB10 hybrid film, where the inset shows the same area under higher magnification. (f) Element mapping of aluminum via EDS in the SFF90−GB10 hybrid. (g) Out-of-plane (left) and in-plane (right) WAXS diffraction patterns of the SFF90−GB10 hybrid showing CNF orientation, where the inset illustrates the direction of the incident X-ray. (h) Optical transmittance and haze values of the 50 μm thick hybrid films as a function of gibbsite content at 600 nm wavelength. (i) Pictures of the hybrid samples at various gibbsite loadings.

and styrene−butadiene rubber (SBR), both have room for improvement in terms of material properties and safety, creating an incentive for their replacement with fully bio-based alternatives such as CNFs.[30] Aside from being bio-based and made from renewable sources, a CNF−graphite hybrid with a strong inter-connected CNF network structure can potentially provide paper-like flexibility while limiting the negative effects of volume changes during high cycling rates, essentially making synthetic binders obsolete.[31] Moreover, using SFFs to prepare functional hybrid materials opens up new possibilities for recyclability thanks to the reversible nature of this hemiacetal-based CNF association.[32]

In the present contribution, a novel and scalable materials processing platform for rapid preparation of nanopapers and functional CNF hybrids through a pH-responsive self-assembly mechanism is reported. The applications of these hybrids are then demonstrated in terms of gas barrier, flame retardancy, and energy storage features. We studied the self-assembly of chemically nanofibrillated SFFs and used them to prepare strong proof-of-concept CNF−gibbsite hybrids with gas barrier and fire retardant functionalities. The structure−process−property relationship in these hybrid materials was carefully established. The resulting CNF−gibbsite hybrids exhibited exceptional oxygen barrier properties at 5 wt % gibbsite and an enhanced thermal stability along with self-extinguishing features at 20 wt % gibbsite loading. In order to extend the application of the pH-responsive self-assembly mechanism, the same concept was applied to prepare paper-like CNF−graphite hybrids to be used as bio-based recyclable Li-ion battery electrodes. It was found that with 90 wt % graphite loading these electrodes exhibit a matching electrochemical performance to their commercial equivalents. Moreover, the prepared electrodes could be easily disintegrated and reformed into second-generation electrodes that matched the initial performance, thus demonstrating a potential green pathway for battery reuse and recycling.

RESULTS AND DISCUSSION

Nanofibrillation and Self-Assembly of CNFs. A simple and energy-efficient chemical nanofibrillation method (pH-induced self-fibrillation) followed by a rapid self-assembly strategy was used to first obtain CNFs and then reform them into CNF nanopapers or CNF hybrids using vacuum filtration (Figure 1a). To prepare these materials, aqueous suspensions

https://doi.org/10.1021/acsanm.2c01530
ACS Appl. Nano Mater. 2022, 5, 9188−9200

Table 1. Effects of Gibbsite Content and Dewatering pH on the Degree of Orientation and Mechanical Properties of the CNF−Gibbsite Hybrids[a]

gibbsite content [wt %]	dewatering pH	dewatering time [min]	degree of CNF orientation	degree of gibbsite orientation	tensile strength [MPa]	Young's modulus [GPa]	strain to failure [%]
0	2.5	12	0.68		150 (8)	17.3 (1.3)	1.15 (0.12)
5	2.5	9	0.74	0.90	140 (4)	17.6 (0.8)	1.03 (0.05)
10	2.5	7	0.70	0.89	131 (5)	17.4 (1.1)	0.91 (0.07)
20	2.5	5	0.66	0.87	126 (4)	21.4 (1.1)	0.88 (0.07)
0	4.0	300	0.81		180 (2)	21.3 (0.6)	1.38 (0.06)
10	4.0	255	0.79	0.91	170 (4)	21.9 (0.3)	1.30 (0.10)

[a]Standard deviations are given in parentheses.

of SFFs were chemically nanofibrillated into CNFs at pH = 10.5 (with or without the ensuing second component addition), from which the pH was lowered to 2.5 to perform the self-assembled entrapment of functional materials and rapid dewatering. This approach builds upon our previous work regarding SFFs, combining pH-induced self-fibrillation with a subsequent self-association and rapid processing into films. Using only water-based modification protocols with high potential for practical applicability,[33,34] that is 2,2,6,6-tetramethyl-1-piperidinyloxy (TEMPO) and periodate oxidation, ordinary lignocellulosic fibers are furnished with carboxyl and aldehyde groups to obtain SFFs (Table S1). The unique pH-responsive behavior of CNFs produced from SFFs is attributed to the highly dynamic nature of hemiacetal cross-links together with the electrostatic repulsion induced by the carboxyl groups.[35,36] The combination of these functional groups facilitates the reversible assembly and disassembly of the constituents in aqueous conditions via a simple pH change (Figure 1b,c). This allows a good control of the interactions between CNFs and their nanostructures, ultimately enabling simultaneous extraction and processing of CNFs into 50 μm thick nanopapers in 12 min (Figure 1d).

Structure−Process−Property Relationship in CNF−Gibbsite Hybrids. Incorporation of gibbsite into the CNF dispersion prior to pH-induced self-assembly results in strong, transparent, and homogeneously distributed CNF−gibbsite hybrids. Moreover, CNF−gibbsite hybrids could be dewatered and formed faster than the CNF-only nanopapers. This synergy is attributed to both the charge and dimensions of the gibbsite, combined with the pH-responsive self-associative properties of the CNFs. Accordingly, gibbsite was chosen as the hybrid component for several reasons. First, it was hypothesized that its charge reversal capabilities could be utilized during mixing, especially considering that the isoelectric point of gibbsite coincides well with the nanofibrillation pH of SFFs. Once the negatively charged CNFs are liberated at pH = 10.5, addition of gibbsite, which is also negatively charged at this pH, helps maintain colloidal stability and homogeneous mixing of the components.[37] Subsequently, lowering the pH of this mixture below 10 and reversing the charge of gibbsite (from negative to positive) promotes its association with the negatively charged CNFs through electrostatic interactions.[23] These strong interactions over a wide pH interval (Figure S1) result in the homogeneous inclusion of gibbsite particles by CNFs. However, owing to the anisotropy of the CNFs, the CNF−gibbsite interactions do not result in a macroscopic aggregation, as the components most likely create a volume spanning arrested state that maintains the initial homogeneous component distribution.[38]

Further lowering the pH to 2.5, facilitates faster dewatering via a combination of factors such as protonation of the carboxyl groups,[39] self-balancing of the charges on CNFs and gibbsite,[38] and lowering of cellulose affinity to water through formation of inter- and intra-hemiacetal linkages.[40] Indeed, the dewatering time of CNF−gibbsite hybrids decreases proportionally to the amount of gibbsite (GB) added, where 20 wt % gibbsite (SFF80−GB20) results in 2.5 times faster dewatering (from 12 to 5 min) compared to CNF nanopapers (Figure 2a). Moreover, when the same formulation of CNFs was filtered without any addition of gibbsite (SFF80−GB0), the suspension still took more than 10 min to dewater despite having 20% less material present. This further supports the favorable CNF−gibbsite interactions and their effects on dewatering. To the best of our knowledge, this is the first time a reinforcing clay is also utilized as a dewatering aid during the preparation of homogeneous CNF hybrids. Strong CNF−gibbsite interactions are also reflected in the mechanical properties of the hybrids (Figure 2b).

An increasing Young's modulus (E) can be observed with the increased gibbsite content (from 17 GPa at 0 wt % gibbsite to 21.5 GPa at 20 wt % gibbsite), which is presumably due to the higher modulus of the gibbsite, the high degree of orientation, and the homogeneous distribution of the components within the hybrid structure. While the effects of gibbsite addition on E is rather insignificant at lower gibbsite contents, these effects are magnified to substantial levels at 20 wt % gibbsite, showing an improvement of 26% in modulus. The tensile strength of the hybrid films decreased only slightly with increasing gibbsite content (from 150 MPa at 0 wt % gibbsite to 126 MPa at 20 wt % gibbsite), suggesting that the failure is mostly stress controlled and is likely related to debonding at the interface.[41] Strain-to-failure decreases slightly with increasing gibbsite content (from 1.1% at 0 wt % gibbsite to 0.9% at 20 wt % gibbsite), as is to be expected from the reduced fraction of the relatively more ductile CNF phase (Figure 2c).

The high homogeneity and the layered orientation of the CNF−gibbsite hybrids can be visualized by SEM, X-ray energy-dispersive spectroscopy (EDS) and wide-angle X-ray scattering (WAXS). SEM images clearly show a layered structure, where the gibbsite platelets appear to be embedded within the CNF matrix (Figure 2d), and it is also possible to see the extensive CNF coverage of the gibbsite platelets (Figure 2e). Furthermore, EDS shows the homogeneous distribution of clay within the hybrid structure (Figures 2f, S2 and S3). WAXS analysis provides information about the orientation of the CNF−gibbsite hybrid components, thus further elucidating the structure−process−property relationship. The 2D diffraction patterns of the hybrids exhibit

https://doi.org/10.1021/acsanm.2c01530
ACS Appl. Nano Mater. 2022, 5, 9188−9200

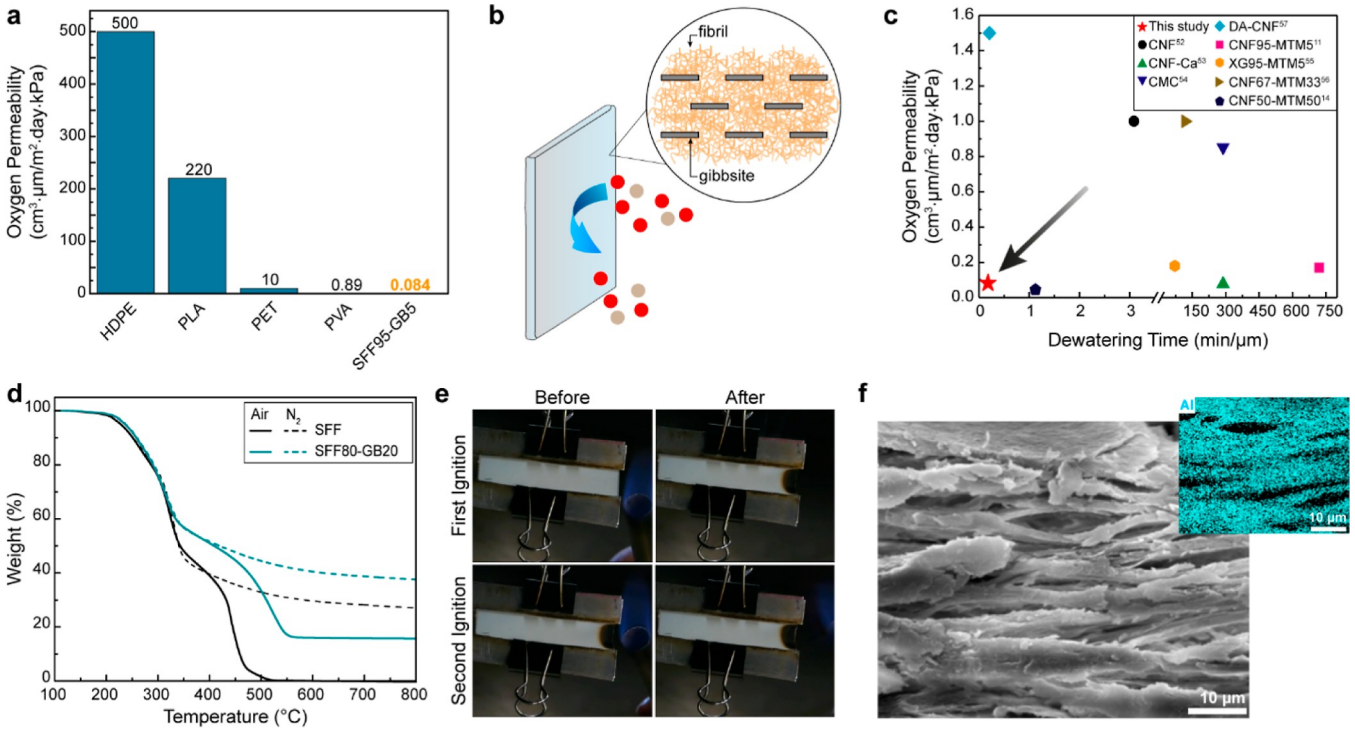

Figure 3. (a) Oxygen permeability of the high barrier SFF95−GB5 at 50% RH compared with conventional plastics (HDPE: high-density polyethylene,[49] PLA: polylactic acid,[50] PET: polyethylene terephthalate,[49] PVA: polyvinyl alcohol[51]) used in packaging. (b) Schematic of the proposed layered structure providing the tortuous pathway for high barrier properties. (c) Graphical comparison of oxygen permeability and dewatering time normalized by thickness for SFF95−GB5 and other comparable wood-based materials reported in the literature (MTM: montmorillonite, XG: xyloglucan, DA-CNF: dialcohol CNF). (d) TGA of SFF and SFF80−GB20 in nitrogen and in air showing the slightly increased thermal stability and char formation in the hybrid. (e) Photographs showing the flame retardant properties of SFF80−GB20 taken before and after the first and second ignition. (f) Cross-sectional SEM and EDS images of the flame-treated SFF80−GB20.

uniform diffraction rings out-of-plane, indicating a random orientation in the film surface, whereas diffraction arcs characteristic of the preferred in-plane orientation can be seen in the cross section (Figures 2g and S4). These observations agree with the previous findings, as CNFs and gibbsite are expected to be predominantly oriented in-plane because they are deposited in a flat conformation during vacuum filtration.[42] Degree of orientation calculations reveal critical information regarding the effects of CNF−gibbsite interactions and processing parameters on the final properties of these hybrids (Table 1). The addition of gibbsite in small amounts (<10 wt %) increases the in-plane orientation of CNFs, which is consistent with our hypothesis of CNF−gibbsite interactions and self-assembly as well as the previously reported literature.[43] The effect of gibbsite on CNF orientation becomes less pronounced at higher gibbsite loadings. This could be attributed to the mutual screening of surface charges by the two oppositely charged materials that results in a fast, but rather imperfect stacking, creating nanoscale porosity[44] that could be further amplified during drying.[23] In fact, total porosity calculated from the weight and dimensions of the hybrid samples shows that the porosity increases with increasing gibbsite loading (Figure S5).

To investigate the role of the charged groups, dewatering of CNF−gibbsite hybrids was performed at pH = 4 (instead of pH = 2.5), where the carboxyl groups on CNFs are partially deprotonated.[39] Processing at pH = 4 not only led to a substantial increase in CNF in-plane orientation (20% higher degree of orientation) but it also improved the mechanical properties of the hybrids (30% improvement in tensile strength, 26% improvement in modulus, and 43% improvement in strain-to-failure for the SFF90−GB10 sample). The degree of orientation of gibbsite remained relatively unchanged despite the change in pH, indicating the relative significance of CNF orientation on the overall mechanical properties of the hybrid. Despite the higher degree of orientation and improved mechanical properties, dewatering of these hybrids at pH = 4 took more than 5 h, thus making them impractical for scale-up and the context of this study (Table 1). However, these observations are valuable as they show the significance of nanoscale orientation and the trade-off between nanostructure and processing time when targeting overall material properties.

CNF−gibbsite hybrids also exhibit high transparency, particularly at lower gibbsite loadings, further indicating well-oriented and well-dispersed gibbsite platelets within the hybrid structure (83% total transmittance for SFF95−GB5 at 50 μm thickness) (Figure 2h,i). The total transmittance of the samples decreases as a function of gibbsite content, which can be attributed to the refractive index of the gibbsite nanoplatelets and pores within the structure acting as scattering centers.[45,46] The increased light scattering within the hybrids also results in a higher haze (from 46% for SFF to 73% for SFF80−GB20 at 600 nm wavelength).

CNF−Gibbsite Hybrids with Gas Barrier and Flame Retardant Functionalities. Thin films (~50 μm) with high transparency and barrier properties are the key components for a variety of applications such as flexible electronics and food packaging.[47] Consequently, synthetic polymers are dominant in these fields due to their simple processing and good barrier properties. While CNF films have been regarded as bio-based

https://doi.org/10.1021/acsanm.2c01530
ACS Appl. Nano Mater. 2022, 5, 9188−9200

and renewable alternatives to these polymers, their often inferior performance (under humid conditions) and long processing times have been the major obstacles against CNFs' scalable implementation. Traditionally, polymer films incorporated with aligned high aspect ratio clays have been shown to enhance their barrier properties through an increased diffusion path for the diffusing gas molecules, often referred to as the tortuous pathway.[48] The same concept can be applied to cellulosic materials (e.g., CNFs) for obtaining bio-based and renewable hybrid films with good barrier properties, provided that they can be processed rapidly and that the components are well-distributed with a sufficient level of alignment. With favorable chemistry (i.e., containing aldehydes capable of forming dynamic hemiacetal cross-links at lower pH values), tunable nanostructure, and fast processing, CNF−gibbsite hybrids are potentially viable ecofriendly packaging materials (Figure S6).

Among the CNF hybrids, SFF95−GB5 with 5 wt % gibbsite, displayed the best oxygen barrier properties with an oxygen permeability value of 0.084 cm^3 μm m^{-2} day^{-1} kPa^{-1} at 50% relative humidity (RH), performing better than the currently available synthetic plastics used in packaging applications (Figure 3a).[49−51] The low oxygen permeability of these hybrids can most probably be explained by their nanostructure. SFF95−GB5 has the highest degree of orientation and the lowest oxygen permeability indicating that there is a sufficient amount of well-distributed gibbsite platelets to create an effective tortuous pathway (Figure 3b). Examining the relative efficiency of the CNF hybrid formation by comparing processing time (normalized by thickness) and barrier performance with those previously reported for wood-based materials shows the potential scalability of these materials. Specifically, SFF95−GB5 hybrids outperform almost all comparable cellulose or hemicellulose-based films in terms of oxygen permeability and its dewatering is drastically faster than similar films reported in the literature (Figure 3c).[11,14,52−57] Moreover, SFF95−GB5 exhibits good mechanical (140 MPa tensile strength, 17.6 GPa Young's modulus, 1.03% strain-to-failure) and optical (83% transmittance) properties along with exceptionally fast papermaking type of processing (9 min dewatering), all of which make it an attractive bio-based candidate for competing with oil-based plastics in packaging applications.

Aside from gas barrier functionality, inorganic components such as gibbsite can furnish CNF materials with other properties such as fire retardancy, thermal stability, and smoke suppression. Such ecofriendly fire retardant materials can be useful in vehicle or building interiors, providing self-extinguishing features that can be critical in life-threatening situations such as domestic fires. Furthermore, because current halogenated flame retardants are often regarded as being environmentally hazardous due to their bioaccumulation and release of toxic byproducts when oxidized, ecofriendly and bio-based fire retardants could be beneficial on multiple levels. The flame retardant behavior of such hybrid materials can be attributed to the layered nanoscale structure with preferential in-plane orientation, resulting in a multitude of CNF−clay interfaces. These abundant interfaces promote char formation under flame exposure and the layered structure of the distributed clay limits diffusion of oxygen and flammable volatiles that result from polymer decomposition.[58] Considering that SFFs and their self-assembled network formation allows rapid processing of highly oriented CNF−gibbsite hybrids with nanoscale structure, the flammability properties of these bio-based and renewable hybrids can be of significant interest. Therefore, we investigated the thermal and thermo-oxidative stability of our CNF−gibbsite hybrids via thermogravimetric analysis (TGA) in nitrogen and air, respectively (Figure 3d).

Thermal decomposition of cellulose occurs through the depolymerization of glycosyl units to volatile products such as levoglucosan, and at the same time, the dehydration of the same units to produce a thermally stable char (35%). In air, the so-produced char is then oxidized to CO and CO_2 in the 400−500 °C range leaving no residue. Such decomposition pathways appeared to be insensitive to gibbsite incorporation. The presence of this latter mainly contributes to an increased final residue as well as a slightly improved stability to high temperature oxidation as demonstrated by the shift of the second weight loss step of SFF80−GB20 in air. SFF80−GB20 also exhibits self-extinguishing characteristics despite containing only 20 wt % gibbsite, as demonstrated by flame tests. Upon direct exposure to methane flame in a horizontal configuration, the hybrid prevents flame propagation to a large extent and the flame self-extinguishes immediately after the source is withdrawn (videos are available in the Supporting Information). Subsequent reapplication of the flame does not ignite the hybrid film owing to the formation of a coherent and flame retardant char residue (Figure 3e). Furthermore, SFF80−GB20 mostly maintains its original shape during and after exposure to the flame. This behavior is in strong contrast with conventional polymers, for which the melt-dripping phenomenon (i.e., the release of molten flaming droplets) can occur and contribute to the spreading of the fire.[59]

Fire retardancy and thermal stability of the SFF80−GB20 is presumably a result of the highly dispersed and well-oriented layered gibbsite phase, which promotes the formation of thermally stable organic−inorganic structures. These structures essentially hinder the release of decomposition products that feed the flame, thus the combustion cannot be sustained and the flame extinguishes.[60] Cross-sectional SEM and EDS images of the treated hybrids support this assumption as they show the formation of expanded microscale voids resulting from the release and entrapment of cellulose decomposition products (Figure 3f). Similar expanded structures have been demonstrated to produce good thermal shielding features for supporting materials coated with such films.[61] Flame retardant SFF80−GB20 combines good mechanical properties (126 MPa tensile strength, 21.4 GPa Young's modulus, 0.88% strain-to-failure) with fast processing (5 min dewatering) and shows that SFFs and their self-assembled fibrillar networks can be used to produce scalable ecofriendly alternatives to conventional flame retardants.

CNF−Graphite Hybrids as Recyclable Li-Ion Battery Electrodes. To extend the applications of SFFs and their self-assembled structures for the preparation of advanced materials, CNF−graphite hybrids with high loadings of graphite (>85 wt %) were prepared. Such materials typically find use as anodes for Li-ion batteries, using graphite's ability to reversibly store and release Li^+ through the well-understood intercalation chemistry.[62] Commercial Li-ion anodes are made from aqueous slurries of graphite that are blade-coated onto a copper foil acting both as a mechanical support and a current collector. As commercial anodes must have a high loading of active material, their preparation necessitates the use of binders (e.g., CMC and SBR), which help disperse graphite in water

https://doi.org/10.1021/acsanm.2c01530
ACS Appl. Nano Mater. 2022, 5, 9188−9200

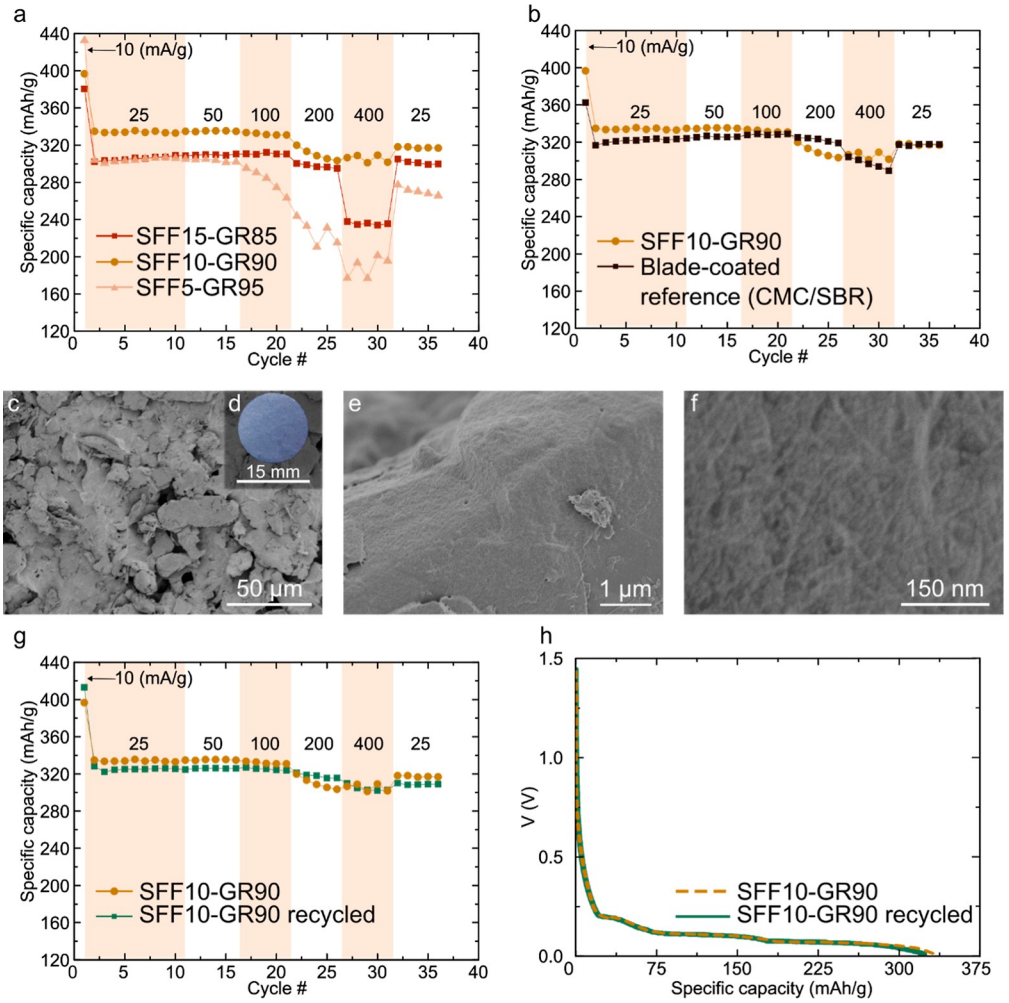

Figure 4. (a) Rate capability profiles of the CNF−graphite hybrids (SFF15−GR85, SFF10−GR90, SFF5−GR95) as Li-ion anodes [measured against Li metal, with a 1 M $LiPF_6$ ethylene carbonate (EC)/dimethyl carbonate (DMC) (1:1 vol %) electrolyte]. (b) SFF10−GR90 hybrid anode compared to a blade-coated reference (made with 2.5 wt % of CMC and 2.5 wt % SBR as binder). (c) Low-magnification SEM micrograph and (d) photograph of an SFF10−GR90 hybrid anode. (e) SEM micrograph of an SFF10−GR90 hybrid and (f) section of the same area shown under higher magnification. (g) Rate capability profile of an SFF10−GR90 anode compared to that of a recycled second-generation SFF10−GR90 anode. (h) Discharge profiles of SFF10−GR90 hybrid anodes and their recycled versions, showing their lithiation at 25 mA/g.

and provide the blade-coated electrodes with good mechanical properties. Owing to their high aspect ratio, CNFs can form strong, entangled network structures at low additions and could presumably be utilized as a fully bio-based binder for high loading graphite electrodes. Furthermore, the distinct chemistry of CNFs obtained from SFFs makes them particularly interesting in the preparation of graphite composites. Specifically, previous studies have shown that carboxyl-bearing CNFs can efficiently disperse carbon rich micro- and nanoparticles in water[63] and aldehydes are known to adsorb onto graphitic surfaces.[64] Consequently, CNF−graphite hybrids (SFF−GR) were prepared using the same strategy as for CNF−gibbsite hybrid films, defined as SFF15−GR85, SFF10−GR90, SFF5−GR95, showing the relative amounts of each component in wt %. These suspensions all showed remarkably short dewatering times (<3 min), which is comparable to the processing time typically associated with the blade coating and drying of commercial electrodes.

The cycling properties of the CNF−graphite hybrids largely differ based on their composition (Figure 4a). These plots, known as rate-capability curves, display the specific capacity (spC, charge stored per weight of active material) of the electrode as they are cycled at different rates. Both SFF15−GR85 and SFF10−GR90 hybrids showed stable cycling behavior. The drop in specific capacity at rates over 200 mA/g is typical for graphite anodes[65] and is associated with the kinetic limitations of the transport of Li^+ in the electrode. SFF10−GR90 anodes showed a higher spC than SFF15−GR85 anodes (about 330 and 300 mA h/g at low rates, respectively). This difference is most likely due to the higher content of CNFs in SFF15−GR85, which are electrically insulating and as such prevent an efficient charge transfer within the electrode. SFF5−GR95 anodes showed very poor cyclability at high rates with a much larger drop in spC. As graphite undergoes lithiation/delithiation, it swells/shrinks by about 10%. Consequently, the binder network must be strong enough to prevent the electrode from undergoing irreversible structural damages at high rates. For SFF5−GR95 hybrids, the CNF weight fraction is presumably too low to form a strong network to protect the electrode's structure upon cycling. Additionally, the SFF5−GR95 anodes also showed poor recovery in spC (comparing the cycles at 25 mA/g rate before and after the high-rate cycling), further indicating that the

https://doi.org/10.1021/acsanm.2c01530
ACS Appl. Nano Mater. 2022, 5, 9188−9200

electrode's structure has been damaged when cycled at a high rate.

Based on these observations, the hybrids with 90 wt % graphite appeared to outperform the other formulations and were thus further characterized by comparing their performance to those of conventionally prepared reference electrodes. The results indicate that at comparable graphite loadings (8.5 mg/cm^2), the cycling performance of SFF10−GR90 hybrids are on par with blade-coated reference electrodes prepared using commercial binder solutions (CMC and SBR) (Figure 4b). The good cycling properties of these freestanding CNF−graphite hybrids (especially at high cycling rates) can be attributed to their nanoscale morphology, consisting of graphite particles held together by a strong and well-distributed CNF network (Figure 4c,d). Indeed, high magnification SEM images show that the surface of the graphite particles is covered with a microscale smooth film (Figure 4e) consisting of nanofibrillated SFFs (Figure 4f). The mechanical properties of SFF10−GR90 hybrids are excellent (2.5 MPa tensile strength, 0.83 GPa Young's modulus, 0.35% strain-to-failure) despite containing a low weight fraction of reinforcing CNFs, further supporting the strong binder network hypothesis regarding the remarkable performance of these materials even at high cycling rates (Figures S7 and S8). Consequently, SFF-based CNFs and their pH-responsive self-association allows for rapid preparation of bio-based and renewable CNF−graphite anodes for Li-ion batteries, whereas the reversible nature of this versatile assembly suggests the prospect of recyclability.

As the demand for Li-ion batteries keeps increasing, there is a critical need for better materials and methods for recycling battery components. Considering that most active materials used in Li-ion electrodes, including graphite, are extracted through mining and thus have a certain environmental cost, recyclability of battery components is a significant issue.[66] In fact, because virgin graphite is considered cheaper than recovered graphite, Li-ion electrodes are generally only recycled for their costly metals (e.g., Co and Li).[67] In this respect, pH-responsive CNF−graphite hybrids should be much easier to recycle compared to commercial anodes due to numerous beneficial properties. First, CNF−graphite electrodes do not require the support of a copper foil, which poses a challenge in commercial anodes to separate and recover. Second, the dynamic nature of the hemiacetal cross-links together with the electrostatic repulsion of the carboxyl groups should make it possible to easily re-disperse the used anodes by liberating the graphite from the CNF network under slightly basic aqueous conditions (pH = 8). Finally, and perhaps most importantly, based on the reversible interaction between CNFs (Figure 1c), these dispersions could possibly be reformed into second-generation anodes.

To demonstrate potential recyclability, electrodes from the used batteries were removed, washed, disintegrated, and used to prepare new anodes following the same method for the initial electrodes. When submitted to the same rate capability measurements as the virgin electrodes, the recycled electrodes showed nearly identical properties to the virgin electrodes (Figure 4g). On average, the recycled electrodes presented spCs marginally lower (3−5%) than their virgin counterparts, demonstrating that neither use nor recycling steps caused any significant damage to the graphite particles or CNFs in the electrodes. This observation is further supported by the identical discharge profiles of the original and recycled electrodes (Figure 4h). SEM micrographs of the recycled samples (Figure S9) further indicate that the employed fabrication method was successful in reforming the CNF binder network, which is necessary for the mechanical and electrochemical performance of the recycled second-generation electrode. These results illustrate that our SFFs and their self-assembled fibrillar networks enable rapid processing of renewable and fully recyclable graphite anodes for Li-ion batteries.

CONCLUSIONS

A new, scalable materials processing platform for the rapid preparation of nanopapers and functional cellulose hybrids was demonstrated. Subsequently, the applications of these hybrids were shown in terms of gas barrier, flame retardancy, and energy storage features. Specifically, pH-responsive CNF networks were produced from self-fibrillating cellulose fibers, which were self-assembled with functional nano- and micromaterials. This novel method relies on the favorable chemistry of self-fibrillating cellulose fibers, where the CNFs can be simultaneously liberated and processed with other components to rapidly produce advanced functional materials using a scalable procedure similar to papermaking. Strong CNF−gibbsite hybrid films with homogeneous clay distribution were obtained in less than 10 min, owing to careful tailoring of component interactions to achieve a nacre-mimetic layered structure. It was shown that processing parameters, such as pH, dewatering speed, and clay content, govern the degree of orientation and the overall material properties in these hybrids. At 5 wt % gibbsite, these rapidly processed (9 min dewatering) hybrids are strong, transparent, and exhibit exceptional oxygen barrier properties (0.084 cm^3 μm m^{-2} day^{-1} kPa^{-1} at 50% RH). At 20 wt % gibbsite, the hybrids show improved thermal stability and self-extinguishing properties with good mechanical integrity and even faster processing times (5 min dewatering) indicating they have potential as scalable bio-based alternatives to conventional flame retardants. Utilizing the same processing concept, freestanding CNF−graphite electrodes with high graphite loadings (90 wt % graphite) were obtained. These hybrids were processed rapidly (3 min dewatering) into Li-ion battery electrodes and matched the electrochemical performance and processing speed of commercially available graphite anodes made with commercial binder solutions. Furthermore, these electrodes can be fully recycled and reformed into second-generation electrodes, while maintaining their initial performance, thus potentially opening new pathways for battery recycling. This versatile methodology for the preparation of functional hybrids combines a bio-based and sustainable manufacturing strategy with excellent processing speed and high material performance, which overall shows large promise for scalable processing of advanced ecofriendly materials.

MATERIALS AND METHODS

Materials. Bleached, industrially-refined, never-dried softwood kraft pulp fibers (Norwegian spruce and Scots pine mixture) were obtained from BillerudKorsnäs AB (Gruvön pulp mill, Grums, Sweden). Sodium hypochlorite (10−15% solution), TEMPO (free radical), hydroxylamine hydrochloride, sodium bromide, sodium (meta)periodate (99%), 2-propanol (99.9%), aluminum-tri-*sec*-butoxide (97%), graphite (powder, <20 μm, synthetic), lithium hexafluorophosphate electrolyte (1.0 M LiPF6 in 50/50 v/v EC/DMC, battery grade), and lithium foil (19 mm thickness, 99.9%

https://doi.org/10.1021/acsanm.2c01530
ACS Appl. Nano Mater. 2022, 5, 9188−9200

purity) were all purchased from Sigma-Aldrich and were used as received. Sodium hydroxide and hydrochloric acid standard solutions (1 M) were obtained from Merck Millipore. Carbon black (Super P), CMC (degree of substitution 0.8), copper foil (9 μm thickness) and coin cell parts were purchased from MTI (Delhi, India). SBR was purchased from Redoxme AB (Norrköping, Sweden). Microporous polypropylene separator (Celgard 2500, 25 μm) was purchased from Celgard (Charlotte, NC).

Preparation and Characterization of SFFs. SFFs were prepared via sequential TEMPO−periodate oxidation according to a previously reported procedure.[19] First, TEMPO oxidation was performed using the TEMPO/NaBr/NaClO protocol in water at pH = 10.5.[36] 0.1 mmol TEMPO, 1 mmol NaBr, and 9.7 mmol NaClO per gram of dry fiber were added to a 12 g/L fiber suspension and allowed to react for 1.5 h under gentle stirring at room temperature. The reaction pH was maintained at 10.5 by dropwise addition of NaOH to the suspension. For the subsequent periodate oxidation, 3.0 g of sodium periodate was added per gram of dry TEMPO-oxidized fiber to a 12 g/L fiber suspension under gentle stirring. To limit side reactions, the fibers were oxidized for 24 h at room temperature in the dark, and 6.3 vol % 2-propanol was added to the suspension as a radical scavenger. Both reactions were terminated by filtration and thorough washing with deionized (DI) water.

The total charge of the SFFs was determined via conductometric titration using a Metrohm 702 SM Titrino titrator, according to the SCAN-CM 65:02 standard. Each measurement was performed in triplicate. The aldehyde content was determined by titration with NaOH after reaction with hydroxylamine hydrochloride, which reacts with the aldehydes to release a stoichiometric amount of protons.[68] pH-responsive nanofibrillation and self-assembly of SFFs were monitored by measuring the turbidity of 30 mL SFF dispersions (2 g/L) at different pH values using a Hach 2100AN IS turbidimeter (Loveland, CO). Self-assembly of chemically nanofibrillated SFFs were observed via AFM. AFM images were collected using a MultiMode 8 (Bruker, Santa Barbara, CA) in tapping mode with RTESPA-300 cantilevers having a resonant frequency of 300 kHz and a spring constant of 40 N/m. Nanofibrillated SFFs were spin-coated onto clean silica wafers pretreated with poly(allylamine hydrochloride) at different pH values.

Preparation of Gibbsite. Aluminum-tri-*sec*-butoxide was used as a precursor in gibbsite preparation according to a previously reported protocol.[69] 0.16 M of aluminum-tri-*sec*-butoxide was dissolved in 500 mL of 0.05 M HCl and the turbid suspension was stirred vigorously at room temperature in a closed container for 18 h. Then, the temperature was increased to 55 °C and mixing was continued for another 6 h to perform hydrolysis and peptization. After this, stirring was stopped and the solution was heated in an oven at 85 °C for 72 h. Finally, the suspension was dialyzed against DI water using a 14,000 kDa cutoff membrane tube to remove the unreacted precursor and the resulting suspension (0.43 wt % gibbsite) was stored at room temperature.

Characterization of Cellulose−Gibbsite Interactions. SFF−gibbsite interactions were monitored over a pH range of 2−12 using a quartz crystal microbalance with dissipation (QCM-D) with a method similar to a previously reported protocol.[70] SFFs were chemically nanofibrillated and spin-coated onto clean QCM quartz crystals with 50 nm thick SiO_2 layer (QSX303) that had been saturated with an anchoring layer of polyvinylamine. Similarly, model cellulose films were also prepared as reference using a procedure similar to a one established earlier. QCM crystals spin-coated with cellulose were washed with Milli-Q water and dried with a gentle flow of nitrogen until the measurements were performed. Cellulose−gibbsite interactions were studied using QCM-D equipment (QCM-E4, Q-Sense AB, Göteborg, Sweden) at room temperature with a flow rate of 0.15 mL/min. Baseline was established by running Milli-Q water and then gibbsite (0.05 g/L) was adsorbed on cellulose spin-coated crystals at pH = 2. After gibbsite adsorption, the pH in the measurement cell was adjusted incrementally (2−12) with intermediate rinsing steps (5 mM NaCl) and the status of the adsorbed gibbsite was monitored continuously.

Preparation of Cellulose Hybrids. SFF−gibbsite hybrids with different compositions (1, 5, 10, and 20 wt % gibbsite) were prepared as follows. An unfibrillated SFF dispersion containing 10 mM NaCl was brought to pH = 10.5 using 0.1 M NaOH under continuous magnetic stirring to achieve chemical nanofibrillation and obtain CNFs. The pH of the dispersion was maintained at 10.5 for 5 min to ensure homogeneity in the process. Then, gibbsite (0.43 wt %) was added to this CNF dispersion followed by lowering of the pH to 2.5 using 0.1 M HCl under constant stirring to perform the self-assembled inclusion of gibbsite. The final concentration in all mixtures was kept at 4 g/L and the total mixture volume was always 100 mL unless stated otherwise. Afterward, the mixtures were vacuum-filtered using hydrophilic Durapore membranes with a pore size of 0.65 μm to form wet hybrid cakes. Dewatering time was taken as the time it takes from starting the filtration until the formation of a mechanically strong wet cake with no visible water on the surface, after which the wet hybrids were dried immediately in a hand sheet dryer (Rapid Köthen, Austria) under reduced pressure and 93 °C for 12 min to obtain the SFF−gibbsite hybrids (50−60 μm dry thickness). SFF−graphite hybrids with 85, 90, and 95 wt % graphite were also prepared using the aforementioned protocol. These hybrids were prepared with a graphite loading of 8.5 mg/cm^2 and the used graphite contained 1.04 wt % carbon black. Prepared hybrids were then carefully dried (70 °C overnight in a vacuum oven), punched into 15 mm diameter discs, and assembled into Li-ion batteries in a glovebox environment.

Characterization of Cellulose Hybrids. Tensile tests for SFF−gibbsite hybrids were carried out using a Universal Testing Machine (Instron 5944, USA) equipped with a 2 kN load cell (500 N load cell was used for SFF−graphite hybrids) and a video extensometer (AVE). For each composition, 8−10 specimens of 50 mm length and 5 mm width were tested. The gauge length was set to 20 mm, and the strain rate was 0.1 min^{-1}. All samples were preconditioned in a room kept at 23 °C and 50% RH for 48 h. The modulus was determined by fitting a linear curve from the initial elastic region (0.1−0.3% strain). All reported modulus and strength values are statistical average of at least eight samples for each composition. Optical properties were measured using a Shimadzu UV-2550 UV−vis spectrophotometer equipped with an integrating sphere accessory. Measurements were taken at three random points on each sample and performed in triplicate. Oxygen permeability was determined (5 cm^2 exposure area) using a MOCON OX-TRAN model 2/21 according to the ASTM D3985 standard. The measurements were performed in duplicate at 23 °C with 50% and 80% RH using the same RH on both sides of the sample. Water vapor permeability was determined (5 cm^2 exposure area) using a MOCON PERMATRAN-W model 3/33. Measurements were performed in duplicate at 23 °C and 50% RH. Densities of the hybrids were determined experimentally by using the ratio of dry weight and volume of disc-shaped samples, which were punched out to obtain standard circles with 15 mm diameter. Total porosity was then calculated based on the theoretical composite density (1.5 g/cm^3 for cellulose and 2.3 g/cm^3 for gibbsite) using the weight and volume fractions of the components in the hybrids according to eqs S1−S3 where w, v, and ρ are the weight fraction, volume fraction, and density, respectively.[41]

$$\frac{1}{\rho_{\text{th,comp}}} = \sum_{i=1}^{n} \frac{w_i}{\rho_i} \tag{1}$$

$$v_i = w_i \frac{\rho_{\text{th,comp}}}{\rho_i} \tag{2}$$

$$\text{Porosity, } \phi = \frac{\rho_{\text{th,comp}} - \rho_{\text{exp}}}{\rho_{\text{th,comp}}} \tag{3}$$

Wide-Angle X-ray Scattering. The alignment of components in the hybrids were determined by WAXS measurements using an Anton Paar SAXSpoint 2.0 system (Anton Paar, Graz, Austria) equipped with a Microsource X-ray source (Cu Kα radiation, wavelength 0.15418 nm) and a Dectris 2D CMOS Eiger R 1M detector with a 75

https://doi.org/10.1021/acsanm.2c01530
ACS Appl. Nano Mater. 2022, 5, 9188−9200

× 75 μm^2 pixel size. All measurements were performed with a beam size of approximately 500 μm diameter and a beam path pressure of about 1−2 mbar. The sample to detector distance was 111 mm during the measurements. All samples were mounted on a sampler holder for solids 10 × 10 mm^2 (Anton Paar, Graz, Austria). The transmittance was determined and used for scaling of intensities.

The degree of orientation (Π) for cellulose and gibbsite was calculated according to the intensity distributions of the azimuthal angle using the following equation

$$\Pi = \frac{180^\circ - \mathrm{FWHM}}{180^\circ} \quad (4)$$

where FWHM is the full width at half-maximum of the azimuthal angle distribution.

Thermal and Flammability Analyses. Thermal and thermo-oxidative degradation of the hybrids were investigated using TGA. Thermal analyses were performed using a TAQ500 thermogravimetric balance (TA Instruments, South Carolina) in a temperature range of 100−800 °C (heating rate of 10 °C/min) under nitrogen and air atmospheres, respectively. The flame retardant behavior of the hybrids was evaluated using the UL-94 horizontal flame test (ASTM D 4986) with samples (11 × 55 mm) mounted on a horizontal metallic frame. The samples were ignited by a 20 mm methane flame for 3 s and each test was performed in triplicate. Samples were conditioned under 23 °C and 50% RH for 48 h prior to testing.

Battery Assembly. CR2032 coin cells were assembled in a glovebox (MBraun Labstar pro, <0.5 ppm H_2O, <0.5 ppm O_2). Metallic lithium foil and a Celgard separator were punched into 12 and 19 mm discs, respectively. 125 μL of electrolyte (1.0 M $LiPF_6$ in 50/50 v/v EC/DMC) was added dropwise during the assembly. The negative electrode, separator, and positive electrode were stacked in CR2032 stainless-steel cases. In the case of the hybrid electrode, because no copper foil was used in the electrode preparation, a 15 mm stainless-steel disc was used as a current collector. Extra stainless-steel spacers were used to ensure good electrical contact between the electrodes and the case upon closing the battery. Coin cells were sealed using an electric coin cell crimper (YLJ-1-4TA, MTI). Batteries were left to rest for 12 h before cycling.

Preparation of Blade-Coated Electrodes. 2 g of graphite powder was added stepwise to 52.5 mg CMC and 105 mg SBR (50 wt % aqueous dispersion) in 4.35 g of DI water and mixed at 15,000 rpm for a total of 15 min using a high-shear mixer (Ultra-Turrax, IKA). Slurries were blade-coated onto 9 μm thick copper foil using a hand coater. The blade height was adjusted (between 400 and 600 μm) to achieve a dry loading of 8.5 mg/cm^2, thus matching the loading of CNF−graphite hybrids. The coated foils were dried in a vacuum oven (48 h, 70 °C) and punched into 15 mm discs.

Galvanostatic Charge/Discharge Cycling. The electrochemical properties of the graphite electrodes were evaluated by cycling coin cells (graphite working electrodes vs metallic Li reference electrodes) at constant currents. In order to ensure the optimal formation of the solid electrolyte interface, the initial lithiation (discharge) was carried out at a very low rate of 10 mA/g. This step is referred to as F (formation step) in the main text. Graphite electrodes were then submitted to 10 delithiation/lithiation (charge/discharge) cycles at a low rate of 25 mA/g before being allowed to be cycled at higher rates. In order to investigate the electrochemical properties of the graphite electrodes at higher rates, an asymmetric rate capability procedure was used. With this procedure, the graphite lithiation was always carried out at a low rate of 25 mA/g (thus ensuring complete lithiation) while the delithiation rate was gradually increased (50, 100, 200, 400 mA/g). For each delithiation rate investigated, the batteries were cycled five times. This method mimics the behavior of a graphite anode in a commercial battery that would be slowly charged to its maximum capacity, before being discharged at rates that can vary from very low to very high.

Recycling of Cellulose Hybrid Electrodes. Used coin cells were brought inside a glovebox, with their graphite electrodes in the delithiated state. They were carefully uncrimped and the hybrid electrodes were extracted. Next, each electrode was soaked in EC/DMC (10 mL, 1:1 vol %) for 12 h. The used washing solvent was replaced by new EC/DMC and the washing operation was repeated two extra times. The hybrid electrodes were then taken out of the glovebox and soaked in an excess of DI water as a final washing step. After washing, the still intact electrodes were placed in a small beaker filled with DI water and the pH was increased to 8 with 0.01 M NaOH in order to break up the composite structure and re-liberate the components (CNFs and graphite flakes). The suspension was mixed at 10,000 rpm for a total of 5 min using a high-shear mixer (Ultra-Turrax, IKA) to ensure homogeneity. Afterward, pH of the suspension was lowered to 2.5 by adding 0.01 M HCl and the suspension was subsequently dewatered (3 min dewatering) to form the recycled electrode, which was then dried and assembled into a second-generation battery for further cycling.

Scanning Electron Microscopy. Morphology of the hybrids was studied using a field-emission scanning electron microscope S-4800 (Hitachi, Japan). Prior to imaging, all specimens were sputter-coated for 20 s with Pt/Pd (Cressington R208, UK). EDS analysis was carried out to determine the gibbsite distribution in the hybrids using SEM at an accelerating voltage of 7 kV equipped with an X-Max 80 mm^2 detector (Oxford Instruments, UK). Morphology of the post-combustion residues collected from the flame tests were investigated using an EVO15 SEM (Zeiss, Germany) at an accelerating voltage of 20 kV. The specimens were mounted on a conductive tape, where the cross sections of the flame-exposed surfaces were imaged.

■ ASSOCIATED CONTENT

Supporting Information

The Supporting Information is available free of charge at https://pubs.acs.org/doi/10.1021/acsanm.2c01530.

Chemical characterization of the fibers; QCM plots showing component affinities; SEM and EDS images of the SFF−GB hybrids; WAXS diffractograms of the hybrids; density and porosity plots; oxygen and water vapor permeability plots; SEM images of the SFF−GR electrodes; stress−strain curves and discharge plots of the hybrid electrodes; and SEM images of the recycled anodes (PDF)

Flame retardancy test (MP4)

■ AUTHOR INFORMATION

Corresponding Authors

Yunus Can Gorur − *Department of Fibre and Polymer Technology, KTH Royal Institute of Technology, SE-100 44 Stockholm, Sweden;* orcid.org/0000-0003-0519-7917; Email: gorur@kth.se

Lars Wågberg − *Department of Fibre and Polymer Technology, KTH Royal Institute of Technology, SE-100 44 Stockholm, Sweden; Wallenberg Wood Science Center, SE-100 44 Stockholm, Sweden;* orcid.org/0000-0001-8622-0386; Email: wagberg@kth.se

Authors

Hugo S. Francon − *Department of Fibre and Polymer Technology, KTH Royal Institute of Technology, SE-100 44 Stockholm, Sweden;* orcid.org/0000-0002-0534-4633

Jatin Sethi − *Department of Fibre and Polymer Technology, KTH Royal Institute of Technology, SE-100 44 Stockholm, Sweden*

Lorenza Maddalena − *Dipartimento di Scienza Applicata e Tecnologia, Politecnico di Torino, 15121 Alessandria, Italy*

Céline Montanari − *Department of Fibre and Polymer Technology, KTH Royal Institute of Technology, SE-100 44 Stockholm, Sweden; Wallenberg Wood Science Center, SE-*

https://doi.org/10.1021/acsanm.2c01530
ACS Appl. Nano Mater. 2022, 5, 9188−9200

100 44 Stockholm, Sweden; orcid.org/0000-0001-6017-1774

Michael S. Reid − *Department of Fibre and Polymer Technology, KTH Royal Institute of Technology, SE-100 44 Stockholm, Sweden;* orcid.org/0000-0002-0999-6671

Johan Erlandsson − *Department of Fibre and Polymer Technology, KTH Royal Institute of Technology, SE-100 44 Stockholm, Sweden;* orcid.org/0000-0003-1874-2187

Federico Carosio − *Dipartimento di Scienza Applicata e Tecnologia, Politecnico di Torino, 15121 Alessandria, Italy;* orcid.org/0000-0003-4067-503X

Per A. Larsson − *Department of Fibre and Polymer Technology, KTH Royal Institute of Technology, SE-100 44 Stockholm, Sweden;* orcid.org/0000-0002-7410-0333

Complete contact information is available at: https://pubs.acs.org/10.1021/acsanm.2c01530

Notes

The authors declare no competing financial interest.

■ ACKNOWLEDGMENTS

This work has been carried out within the national platform Treesearch and was funded through the strategic innovation program BioInnovation, a joint effort by Vinnova, Formas, and the Swedish Energy Agency. Y.C.G. acknowledges BillerudKorsnäs AB for their direct financial contribution to the project. L.W. acknowledges The Knut and Alice Wallenberg foundation for financial support through the Wallenberg Wood Science Center. The authors would also like to thank Assoc. Prof. Anita Teleman from Research Institutes of Sweden (RISE) for her help in conducting WAXS measurements.

■ REFERENCES

(1) Carosio, F.; Kochumalayil, J.; Fina, A.; Berglund, L. A. Extreme Thermal Shielding Effects in Nanopaper Based on Multilayers of Aligned Clay Nanoplatelets in Cellulose Nanofiber Matrix. *Adv. Mater. Interfaces* **2016**, *3*, 1600551.

(2) Koga, H.; Nogi, M.; Komoda, N.; Nge, T. T.; Sugahara, T.; Suganuma, K. Uniformly Connected Conductive Networks on Cellulose Nanofiber Paper for Transparent Paper Electronics. *NPG Asia Mater.* **2014**, *6*, No. e93.

(3) Gu, H.; Liu, C.; Zhu, J.; Gu, J.; Wujcik, E. K.; Shao, L.; Wang, N.; Wei, H.; Scaffaro, R.; Zhang, J.; Guo, Z. Introducing Advanced Composites and Hybrid Materials. *Adv. Compos. Hybrid Mater.* **2018**, *1*, 1−5.

(4) Cademartiri, L.; Bishop, K. J. M. Programmable Self-Assembly. *Nat. Mater.* **2015**, *14*, 2−9.

(5) Stupp, S. I.; Zha, R. H.; Palmer, L. C.; Cui, H.; Bitton, R. Self-Assembly of Biomolecular Soft Matter. *Faraday Discuss.* **2013**, *166*, 9−30.

(6) Frenkel, D. Order through Entropy. *Nat. Mater.* **2015**, *14*, 9−12.

(7) Barthelat, F. Nacre from Mollusk Shells: A Model for High-Performance Structural Materials. *Bioinspiration Biomimetics* **2010**, *5*, 035001.

(8) Hamedi, M. M.; Hajian, A.; Fall, A. B.; Håkansson, K.; Salajkova, M.; Lundell, F.; Wågberg, L.; Berglund, L. A. Highly Conducting, Strong Nanocomposites Based on Nanocellulose-Assisted Aqueous Dispersions of Single-Wall Carbon Nanotubes. *ACS Nano* **2014**, *8*, 2467−2476.

(9) Sehaqui, H.; Liu, A.; Zhou, Q.; Berglund, L. A. Fast Preparation Procedure for Large, Flat Cellulose and Cellulose/Inorganic Nanopaper Structures. *Biomacromolecules* **2010**, *11*, 2195−2198.

(10) Mattos, B. D.; Tardy, B. L.; Greca, L. G.; Kämäräinen, T.; Xiang, W.; Cusola, O.; Magalhães, W. L. E.; Rojas, O. J. Nanofibrillar Networks Enable Universal Assembly of Superstructured Particle Constructs. *Sci. Adv.* **2020**, *6*, No. eaaz7328.

(11) Wu, C.-N.; Saito, T.; Fujisawa, S.; Fukuzumi, H.; Isogai, A. Ultrastrong and High Gas-Barrier Nanocellulose/Clay-Layered Composites. *Biomacromolecules* **2012**, *13*, 1927−1932.

(12) Yao, K.; Huang, S.; Tang, H.; Xu, Y.; Buntkowsky, G.; Berglund, L. A.; Zhou, Q. Bioinspired Interface Engineering for Moisture Resistance in Nacre-Mimetic Cellulose Nanofibrils/Clay Nanocomposites. *ACS Appl. Mater. Interfaces* **2017**, *9*, 20169−20178.

(13) Carosio, F.; Kochumalayil, J.; Cuttica, F.; Camino, G.; Berglund, L. Oriented Clay Nanopaper from Biobased Components-Mechanisms for Superior Fire Protection Properties. *ACS Appl. Mater. Interfaces* **2015**, *7*, 5847−5856.

(14) Liu, A.; Walther, A.; Ikkala, O.; Belova, L.; Berglund, L. A. Clay Nanopaper with Tough Cellulose Nanofiber Matrix for Fire Retardancy and Gas Barrier Functions. *Biomacromolecules* **2011**, *12*, 633−641.

(15) Tian, W.; VahidMohammadi, A.; Reid, M. S.; Wang, Z.; Ouyang, L.; Erlandsson, J.; Pettersson, T.; Wågberg, L.; Beidaghi, M.; Hamedi, M. M. Multifunctional Nanocomposites with High Strength and Capacitance Using 2D MXene and 1D Nanocellulose. *Adv. Mater.* **2019**, *31*, 1902977.

(16) Sinquefield, S.; Ciesielski, P. N.; Li, K.; Gardner, D. J.; Ozcan, S. Nanocellulose Dewatering and Drying: Current State and Future Perspectives. *ACS Sustainable Chem. Eng.* **2020**, *8*, 9601−9615.

(17) Sethi, J.; Oksman, K.; Illikainen, M.; Sirviö, J. A. Sonication-Assisted Surface Modification Method to Expedite the Water Removal from Cellulose Nanofibers for Use in Nanopapers and Paper Making. *Carbohydr. Polym.* **2018**, *197*, 92−99.

(18) Françon, H.; Wang, Z.; Marais, A.; Mystek, K.; Piper, A.; Granberg, H.; Malti, A.; Gatenholm, P.; Larsson, P. A.; Wågberg, L. Ambient-Dried, 3D-Printable and Electrically Conducting Cellulose Nanofiber Aerogels by Inclusion of Functional Polymers. *Adv. Funct. Mater.* **2020**, *30*, 1909383.

(19) Gorur, Y. C.; Larsson, P. A.; Wågberg, L. Self-Fibrillating Cellulose Fibers: Rapid In Situ Nanofibrillation to Prepare Strong, Transparent, and Gas Barrier Nanopapers. *Biomacromolecules* **2020**, *21*, 1480−1488.

(20) Gorur, Y. C.; Reid, M. S.; Montanari, C.; Larsson, P. T.; Larsson, P. A.; Wågberg, L. Advanced Characterization of Self-Fibrillating Cellulose Fibers and Their Use in Tunable Filters. *ACS Appl. Mater. Interfaces* **2021**, *13*, 32467−32478.

(21) Chemin, M.; Heux, L.; Guérin, D.; Crowther-Alwyn, L.; Jean, B. Hybrid Gibbsite Nanoplatelet/Cellulose Nanocrystal Multilayered Coatings for Oxygen Barrier Improvement. *Front. Chem.* **2019**, *7*, 507.

(22) Zhou, Y.; Chen, C.; Zhu, S.; Sui, C.; Wang, C.; Kuang, Y.; Ray, U.; Liu, D.; Brozena, A.; Leiste, U. H.; Quispe, N.; Guo, H.; Vellore, A.; Bruck, H. A.; Martini, A.; Foster, B.; Lou, J.; Li, T.; Hu, L. A Printed, Recyclable, Ultra-Strong, and Ultra-Tough Graphite Structural Material. *Mater. Today* **2019**, *30*, 17−25.

(23) Martin, C.; Barker, R.; Watkins, E. B.; Dubreuil, F.; Cranston, E. D.; Heux, L.; Jean, B. Structural Variations in Hybrid All-Nanoparticle Gibbsite Nanoplatelet/Cellulose Nanocrystal Multilayered Films. *Langmuir* **2017**, *33*, 7896−7907.

(24) Rosenqvist, J.; Persson, P.; Sjöberg, S. Protonation and Charging of Nanosized Gibbsite (α-Al(OH)3) Particles in Aqueous Suspension. *Langmuir* **2002**, *18*, 4598−4604.

(25) Jodin, M.-C.; Gaboriaud, F.; Humbert, B. Limitations of potentiometric studies to determine the surface charge of gibbsite γ-Al(OH)3 particles. *J. Colloid Interface Sci.* **2005**, *287*, 581−591.

(26) Zhang, X.; Huestis, P. L.; Pearce, C. I.; Hu, J. Z.; Page, K.; Anovitz, L. M.; Aleksandrov, A. B.; Prange, M. P.; Kerisit, S.; Bowden, M. E.; Cui, W.; Wang, Z.; Jaegers, N. R.; Graham, T. R.; Dembowski, M.; Wang, H.-W.; Liu, J.; N'Diaye, A. T.; Bleuel, M.; Mildner, D. F. R.; Orlando, T. M.; Kimmel, G. A.; La Verne, J. A.; Clark, S. B.; Rosso, K. M. Boehmite and Gibbsite Nanoplates for the Synthesis of Advanced Alumina Products. *ACS Appl. Nano Mater.* **2018**, *1*, 7115−7128.

(27) Stieger, G.; Scheringer, M.; Ng, C. A.; Hungerbühler, K. Assessing the Persistence, Bioaccumulation Potential and Toxicity of Brominated Flame Retardants: Data Availability and Quality for 36 Alternative Brominated Flame Retardants. *Chemosphere* **2014**, *116*, 118−123.
(28) Lu, H.; Behm, M.; Leijonmarck, S.; Lindbergh, G.; Cornell, A. Flexible Paper Electrodes for Li-Ion Batteries Using Low Amount of TEMPO-Oxidized Cellulose Nanofibrils as Binder. *ACS Appl. Mater. Interfaces* **2016**, *8*, 18097−18106.
(29) Jabbour, L.; Gerbaldi, C.; Chaussy, D.; Zeno, E.; Bodoardo, S.; Beneventi, D. Microfibrillated Cellulose-Graphite Nanocomposites for Highly Flexible Paper-like Li-Ion Battery Electrodes. *J. Mater. Chem.* **2010**, *20*, 7344−7347.
(30) Melnick, R. L.; Huff, J.; Chou, B. J.; Miller, R. A. Carcinogenicity of 1,3-butadiene in C57BL/6 x C3H F1 mice at low exposure concentrations. *Cancer Res.* **1990**, *50*, 6592−6599.
(31) Mahmood, N.; Tang, T.; Hou, Y. Nanostructured Anode Materials for Lithium Ion Batteries: Progress, Challenge and Perspective. *Adv. Energy Mater.* **2016**, *6*, 1600374.
(32) Codou, A.; Guigo, N.; Heux, L.; Sbirrazzuoli, N. Partial periodate oxidation and thermal cross-linking for the processing of thermoset all-cellulose composites. *Compos. Sci. Technol.* **2015**, *117*, 54−61.
(33) Pierre, G.; Punta, C.; Delattre, C.; Melone, L.; Dubessay, P.; Fiorati, A.; Pastori, N.; Galante, Y. M.; Michaud, P. TEMPO-Mediated Oxidation of Polysaccharides: An Ongoing Story. *Carbohydr. Polym.* **2017**, *165*, 71−85.
(34) Koprivica, S.; Siller, M.; Hosoya, T.; Roggenstein, W.; Rosenau, T.; Potthast, A. Regeneration of Aqueous Periodate Solutions by Ozone Treatment: A Sustainable Approach for Dialdehyde Cellulose Production. *ChemSusChem* **2016**, *9*, 825−833.
(35) Erlandsson, J.; Pettersson, T.; Ingverud, T.; Granberg, H.; Larsson, P. A.; Malkoch, M.; Wågberg, L. On the Mechanism behind Freezing-Induced Chemical Crosslinking in Ice-Templated Cellulose Nanofibril Aerogels. *J. Mater. Chem. A* **2018**, *6*, 19371−19380.
(36) Saito, T.; Kimura, S.; Nishiyama, Y.; Isogai, A. Cellulose Nanofibers Prepared by TEMPO-Mediated Oxidation of Native Cellulose. *Biomacromolecules* **2007**, *8*, 2485−2491.
(37) Fall, A. B.; Lindström, S. B.; Sundman, O.; Ödberg, L.; Wågberg, L. Colloidal Stability of Aqueous Nanofibrillated Cellulose Dispersions. *Langmuir* **2011**, *27*, 11332−11338.
(38) Nordenström, M.; Fall, A.; Nyström, G.; Wågberg, L. Formation of Colloidal Nanocellulose Glasses and Gels. *Langmuir* **2017**, *33*, 9772−9780.
(39) Grignon, J.; Scallan, A. M. Effect of PH and Neutral Salts upon the Swelling of Cellulose Gels. *J. Appl. Polym. Sci.* **1980**, *25*, 2829−2843.
(40) Larsson, P. A.; Kochumalayil, J. J.; Wågberg, L. Oxygen and Water Vapour Barrier Films with Low Moisture Sensitivity Fabricated from Self-Crosslinking Fibrillated Cellulose. *15th Fundamental Research Symposium: Advanced in Pulp and Paper Research*, 2013; Vol. *134* (16), pp 851−866.
(41) Medina, L.; Nishiyama, Y.; Daicho, K.; Saito, T.; Yan, M.; Berglund, L. A. Nanostructure and Properties of Nacre-Inspired Clay/Cellulose Nanocomposites-Synchrotron X-ray Scattering Analysis. *Macromolecules* **2019**, *52*, 3131−3140.
(42) Henriksson, M.; Berglund, L. A.; Isaksson, P.; Lindström, T.; Nishino, T. Cellulose Nanopaper Structures of High Toughness. *Biomacromolecules* **2008**, *9*, 1579−1585.
(43) Mianehrow, H.; Lo Re, G.; Carosio, F.; Fina, A.; Larsson, P. T.; Chen, P.; Berglund, L. A. Strong reinforcement effects in 2D cellulose nanofibril-graphene oxide (CNF-GO) nanocomposites due to GO-induced CNF ordering. *J. Mater. Chem. A* **2020**, *8*, 17608−17620.
(44) Walther, A.; Bjurhager, I.; Malho, J.-M.; Pere, J.; Ruokolainen, J.; Berglund, L. A.; Ikkala, O. Large-Area, Lightweight and Thick Biomimetic Composites with Superior Material Properties via Fast, Economic, and Green Pathways. *Nano Lett.* **2010**, *10*, 2742−2748.
(45) Frka-Petesic, B.; Sugiyama, J.; Kimura, S.; Chanzy, H.; Maret, G. Negative Diamagnetic Anisotropy and Birefringence of Cellulose Nanocrystals. *Macromolecules* **2015**, *48*, 8844−8857.
(46) Shannon, R. C.; Lafuente, B.; Shannon, R. D.; Downs, R. T.; Fischer, R. X. Refractive Indices of Minerals and Synthetic Compounds. *Am. Mineral.* **2017**, *102*, 1906−1914.
(47) Priolo, M. A.; Gamboa, D.; Holder, K. M.; Grunlan, J. C. Super Gas Barrier of Transparent Polymer−Clay Multilayer Ultrathin Films. *Nano Lett.* **2010**, *10*, 4970−4974.
(48) Cussler, E. L.; Hughes, S. E.; Ward, W. J.; Aris, R. Barrier Membranes. *J. Membr. Sci.* **1988**, *38*, 161−174.
(49) Lange, J.; Wyser, Y. Recent innovations in barrier technologies for plastic packaging? a review. *Packag. Technol. Sci.* **2003**, *16*, 149−158.
(50) Trifol, J.; Plackett, D.; Sillard, C.; Szabo, P.; Bras, J.; Daugaard, A. E. Hybrid Poly(Lactic Acid)/Nanocellulose/Nanoclay Composites with Synergistically Enhanced Barrier Properties and Improved Thermomechanical Resistance. *Polym. Int.* **2016**, *65*, 988−995.
(51) Lagaron, J. M.; Catalá, R.; Gavara, R. Structural Characteristics Defining High Barrier Properties in Polymeric Materials. *Mater. Sci. Technol.* **2004**, *20*, 1−7.
(52) Wakabayashi, M.; Fujisawa, S.; Saito, T.; Isogai, A. Nanocellulose Film Properties Tunable by Controlling Degree of Fibrillation of TEMPO-Oxidized Cellulose. *Front. Chem.* **2020**, *8*, 37.
(53) Shimizu, M.; Saito, T.; Isogai, A. Water-Resistant and High Oxygen-Barrier Nanocellulose Films with Interfibrillar Cross-Linkages Formed through Multivalent Metal Ions. *J. Membr. Sci.* **2016**, *500*, 1−7.
(54) Aulin, C.; Gällstedt, M.; Lindström, T. Oxygen and Oil Barrier Properties of Microfibrillated Cellulose Films and Coatings. *Cellulose* **2010**, *17*, 559−574.
(55) Kochumalayil, J. J.; Bergenstråhle-Wohlert, M.; Utsel, S.; Wågberg, L.; Zhou, Q.; Berglund, L. A. Bioinspired and Highly Oriented Clay Nanocomposites with a Xyloglucan Biopolymer Matrix: Extending the Range of Mechanical and Barrier Properties. *Biomacromolecules* **2013**, *14*, 84−91.
(56) Bardet, R.; Reverdy, C.; Belgacem, N.; Leirset, I.; Syverud, K.; Bardet, M.; Bras, J. Substitution of Nanoclay in High Gas Barrier Films of Cellulose Nanofibrils with Cellulose Nanocrystals and Thermal Treatment. *Cellulose* **2015**, *22*, 1227−1241.
(57) Larsson, P. A.; Pettersson, T.; Wågberg, L. Improved Barrier Films of Cross-Linked Cellulose Nanofibrils: A Microscopy Study. *Green Mater.* **2014**, *2*, 163−168.
(58) Carosio, F.; Cuttica, F.; Medina, L.; Berglund, L. A. Clay Nanopaper as Multifunctional Brick and Mortar Fire Protection Coating-Wood Case Study. *Mater. Des.* **2016**, *93*, 357−363.
(59) Sun, P.; Jia, Y.; Zhang, X.; Huang, X. Fire Risk of Dripping Flame: Piloted Ignition and Soaking Effect. *Fire Saf. J.* **2021**, *122*, 103360.
(60) Gilman, J. W. Flammability and Thermal Stability Studies of Polymer Layered-Silicate (Clay) Nanocomposites. *Appl. Clay Sci.* **1999**, *15*, 31−49.
(61) Tabaka, W.; Timme, S.; Lauterbach, T.; Medina, L.; Berglund, L. A.; Carosio, F.; Duquesne, S.; Schartel, B. Bench-scale fire stability testing - Assessment of protective systems on carbon fibre reinforced polymer composites. *Polym. Test.* **2021**, *102*, 107340.
(62) Guerard, D.; Herold, A. Intercalation of Lithium into Graphite and Other Carbons. *Carbon* **1975**, *13*, 337−345.
(63) Hajian, A.; Lindström, S. B.; Pettersson, T.; Hamedi, M. M.; Wågberg, L. Understanding the Dispersive Action of Nanocellulose for Carbon Nanomaterials. *Nano Lett.* **2017**, *17*, 1439−1447.
(64) Phillips, T. K.; Bhinde, T.; Clarke, S. M.; Lee, S. Y.; Mali, K. S.; De Feyter, S. Adsorption of Aldehydes on a Graphite Substrate: Combined Thermodynamic Study of C6−C13 Homologues with a Structural and Dynamical Study of Dodecanal. *J. Phys. Chem. C* **2010**, *114*, 6027−6034.
(65) Asenbauer, J.; Eisenmann, T.; Kuenzel, M.; Kazzazi, A.; Chen, Z.; Bresser, D. The Success Story of Graphite as a Lithium-Ion Anode Material-Fundamentals, Remaining Challenges, and Recent Develop-

https://doi.org/10.1021/acsanm.2c01530
ACS Appl. Nano Mater. 2022, 5, 9188−9200

ments Including Silicon (Oxide) Composites. *Sustainable Energy Fuels* **2020**, *4*, 5387−5416.
(66) McManus, M. C. Environmental Consequences of the Use of Batteries in Low Carbon Systems: The Impact of Battery Production. *Appl. Energy* **2012**, *93*, 288−295.
(67) Fan, E.; Li, L.; Wang, Z.; Lin, J.; Huang, Y.; Yao, Y.; Chen, R.; Wu, F. Sustainable Recycling Technology for Li-Ion Batteries and Beyond: Challenges and Future Prospects. *Chem. Rev.* **2020**, *120*, 7020−7063.
(68) Larsson, P. A.; Gimåker, M.; Wågberg, L. The Influence of Periodate Oxidation on the Moisture Sorptivity and Dimensional Stability of Paper. *Cellulose* **2008**, *15*, 837−847.
(69) Louaer, S.; Wang, Y.; Guo, L. Fast Synthesis and Size Control of Gibbsite Nanoplatelets, Their Pseudomorphic Dehydroxylation, and Efficient Dye Adsorption. *ACS Appl. Mater. Interfaces* **2013**, *5*, 9648−9655.
(70) Aulin, C.; Varga, I.; Claesson, P. M.; Wågberg, L.; Lindström, T. Buildup of Polyelectrolyte Multilayers of Polyethyleneimine and Microfibrillated Cellulose Studied by in Situ Dual-Polarization Interferometry and Quartz Crystal Microbalance with Dissipation. *Langmuir* **2008**, *24*, 2509−2518.

https://doi.org/10.1021/acsanm.2c01530
ACS Appl. Nano Mater. 2022, 5, 9188−9200